Interval observer-based fault detection and isolation for quadrotor UAV with cable-suspended load

Xiaoyuan Zhu, *Member*, *IEEE*, Yuxue Li, Guodong Yin, *Senior Member*, *IEEE*, and Ron J. Patton, *Life Fellow, IEEE*

***Abstract*—This paper proposes an actuator fault detection and isolation (FDI) scheme for quadrotor unmanned aerial vehicle (UAV) with cable-suspended load. First, a linear parameter-varying (LPV) model of quadrotor UAV is established, in which the effects of cable-suspended load are considered. Then, a state boundary-based FDI design is systemically presented. A bank of interval observers is constructed to build the preliminary upper and lower boundaries of system states under healthy conditions, where H_- / H_∞ performance is applied to enhance its robustness against disturbances and sensitivity to faults. Furthermore, a novel updating strategy is further proposed to periodically adjust state boundaries to cope with the effects of varying wind disturbances. Finally, based on the *QDrone* platform, experimental tests under random faults are carried out to verify the effectiveness and performance of the proposed scheme.**

***Index Terms*—Fault detection and isolation, interval observers, state boundary, quadrotor UAV, H_- / H_∞ performance**

I. INTRODUCTION

Quadrotor UAVs are used in various fields such as aerial photography, agriculture, and geographical mapping [1]. Among them, UAV logistics is one of the emerging application areas, which can realize package delivery, firefighting, and post-disaster medical rescue [2], [3]. Compared with transportation modes equipped with grippers or cargo boxes, cable-suspended transportation is more efficient, and it preserves agility without bringing additional body inertia, which is more attractive [4]. However, due to the swing movement of the suspended load, the quadrotor UAV with cable-suspended load has higher demands for flight safety and reliability [5]. Furthermore, quadrotor UAV has inherent under-actuation and strong-coupled characteristics [6]. Thus, prompt fault diagnosis is of great significance to flight safety as well as engineering applications of quadrotor UAVs.

Fault diagnosis methods include model-based and data-driven. Considering that many researchers have studied physical characteristics and operating principles of UAVs in-depth, established mathematical models to describe their behavior, and the fault data acquisition is not trivial, model-based approaches are more attractive [7],[8]. Fault diagnosis can be directly achieved by fault estimation, which can reconstruct the fault signal in real time [9],[10]. However, direct fault estimation generally requires that the fault signal and its derivatives are continuously differentiable [11],[12] and its transient performance is also difficult to guarantee, which would directly affect its accuracy as well as reliability. Thus, state estimation can be used instead to perform preceding fault detection and isolation through residual evaluation to ensure reliable system health monitoring and fault diagnosis. State estimation-based fault detection (FD) can achieve more prompt and accurate abnormality alerts [13]. Observer-based methods can be well integrated with the analysis of system dynamics and be implemented online in real-time, which are extensively used. In [14], a neural adaptive observer-based method was designed to detect actuator and sensor faults of quadrotor UAVs. Cen et. al [15] developed an adaptive Thau observer to estimate system states and generate residuals for actuator FD of quadrotor UAV. For attenuating the effects of inevitable model uncertainties and disturbances, H_∞ performance and L_∞ performance are often applied [16], [17]. While guaranteeing robustness against disturbances, it is also necessary to improve sensitivity to faults. Among methods that consider fault sensitivity and disturbance robustness performances simultaneously, those with H_- / H_∞ performance or H_- / L_∞ performance are more appealing. H_- / H_∞ theory was originally proposed by [18], and gradually developed and employed thereafter [17], [19]. Zhang et. al [20] designed a state observer with H_- / H_∞ performance for achieving steering actuator FD. In [17], a comprehensive H_- / L_∞ fault detector was designed where residual generation and threshold computation are achieved simultaneously.

For systems with multiple actuators, fault isolation (FI) is further needed, which determines the location of the faulty component and facilitates follow-up remedial actions [21]. In [22], a robust state observer was designed to generate residuals, and a scheme of binary logic was proposed to isolate the actuator fault of quadrotor UAV by combining the analysis of residual variation. However, it can only deal with the case of a single actuator fault. It is a more attractive strategy to design a bank of observers and to decouple fault from generated residuals. In [23], an observer bank was designed to detect and isolate sensor faults of quadrotor UAV. Li et. al [24] completed the fault location of a microsatellite attitude control system by a bank of multi-objective nonlinear observers and a fault decouple scheme.

In most state observer-based methods, fault detection and isolation are realized by comparing the consistency of the

This work was supported in part by National key Laboratory of Helicopter Dynamics under Grant 2024-ZSJ-LB-02-01, in part by Jiangsu Provincial Scientific Research Center of Applied Mathematics under Grant No.BK20233002, and in part by National Natural Science Foundation of China under Grant 52172402. (*Corresponding author: Xiaoyuan Zhu*)

Xiaoyuan Zhu, Yuxue Li and Guodong Yin are with the School of Mechanical Engineering, Southeast University, Nanjing 211189, China (e-mail: zhuxyc@gmail.com; yx_li@seu.edu.cn; ygd@seu.edu.cn;)

Ron J. Patton is with the School of Engineering, University of Hull, Cottingham Road, Hull HU6 7RX, U.K. (e-mail: r.j.patton@hull.ac.uk).

measured states with the estimated ones. The basic strategy is to generate a residual and compare it with a predefined threshold to determine whether a fault occurs[11], [17], [25] [26]. In the H_∞ norm-based method, a constant threshold is usually set based on engineering experience [14], [15], which is pragmatic but conservative. In the L_∞ norm-based methods, the threshold is generally in the form of exponential functions, calculated according to initial estimation errors and disturbance boundaries [25], [28], which is not adaptive. In fault location, thresholds need to be set for each observer, and the setting of multiple thresholds makes it more complicated. In addition to methods that directly estimate the state and set thresholds considering the effects of disturbances, fault can be detected and isolated by building the permissible boundaries of states in healthy conditions [29], [30]. The transmission processes of disturbance and uncertainty in the system are contained in the boundary estimation [31], [32]. With estimated state boundaries, fault detection and isolation problems become determining whether the measured states are within the estimated boundaries, without additional setting of thresholds. The methods of state boundary estimation contain interval observer-based methods and set-membership estimation methods [33], [34]. The former is applicable to discrete-time systems, while the latter applies to both discrete-time and continuous-time systems, which is more attractive. Ma et al. [35] introduced an interval-based peak-to-peak residual generator for fault diagnosis. In [36], a hybrid fault isolation method was proposed for wind turbines, which used network-based fuzzy inference system to identify model and detected sensor and actuator fault with a bank of quasi-LPV zonotopic observers. Cao et. al [37] achieved actuator FD of quadrotor UAVs by combining extended state observer and interval observer. Zhu et.al [38] dealt with fault isolation of Takagi-Sugeno fuzzy system, which combined a Luenberger-like H-infinity observer and a zonotope method.

For the quadrotor UAV with cable-suspended load, there are various disturbances, including suspended load swing, parameters uncertainty, sensor noise, and ambient wind disturbance. Commonly, external disturbances and model uncertainty are regarded as total disturbances, for which a global boundary is defined [37], [23]. However, this is conservative. Each disturbance has different characteristics. For disturbances caused by parameter uncertainty and suspended load swing, whose boundaries can be obtained by analyzing the slung-load dynamics, their influence can be analyzed within the interval observer. However, this is not feasible for ambient wind disturbance. Since the wind field varies widely with weather conditions [39], it is difficult to define a disturbance boundary that is applied to all working scenarios. Therefore, it is better to adjust and update the effect of wind disturbance periodically according to the weather conditions.

This paper proposes an allowable state boundary-based actuator fault detection and isolation scheme for the quadrotor UAV with cable-suspended load. The main contributions are as follows.

1. An allowable state boundary estimation-based FDI method is proposed for quadrotor UAV system with cable-suspended load, in which the application of H_-/H_∞ performance allows for a trade-off between robustness against internal disturbance and sensitivity to faults.
2. A bank of interval observers is constructed to generate the preliminary upper and lower state boundaries under healthy conditions, which consider the effects of suspended load on the system dynamics, including exerted external disturbances and resulting parameter uncertainty. Furthermore, a novel strategy is proposed to adaptively adjust and update the state boundaries to cope with the effect of wind disturbance.
3. Based on the *QDrone* platform, plenty of experimental tests under random faults are carried out to verify the effectiveness and performance of the proposed scheme.

The structure of the paper is split into five sections, starting with Section II, which establishes the LPV model of quadrotor UAV with cable-suspended load, and Section III, which introduces the proposed fault detection and isolation scheme in detail. Section IV shows experimental results. Finally, Section V highlights the main conclusions of this work.

Notation. $\mathbb{R}_+$ denotes the sets of positive real numbers. For a vector x, $\|x\|_\infty$ is the L_∞ norm and $\|x\|_2$ is the L_2 norm. $diag([x])$ denotes the diagonal matrix with a vector x as the main diagonal element. For a matrix A, $A^\dagger = A^T(AA^T)^{-1}$ denotes the Moore-Penrose inverse, $A^+ = \max\{0, A\}$, $A^- = A^+ - A$, A^T and $A^\perp$ denote its transpose and orthogonal complement, respectively. I denotes the identity matrix. The Hermitian part of a square matrix A is denoted by $\mathrm{He}(A) := A + A^T$.

II. Problem Formulation

A. Dynamic of quadrotor UAV with cable-suspended load

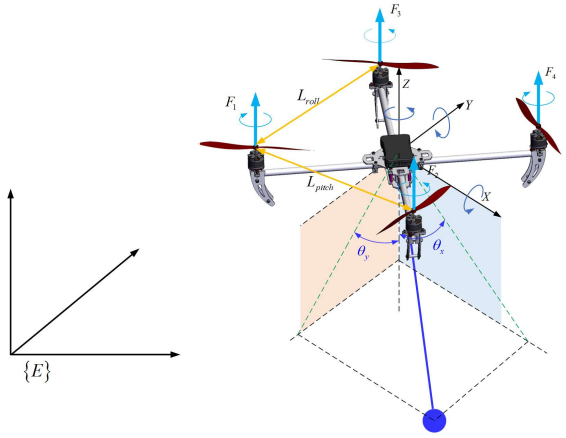

Fig. 1. The quadrotor UAV model with cable-suspended load

The quadrotor UAV with cable-suspended load, shown in Fig. 1, is considered as a three-dimensional point pendulum mass model, satisfying the following assumptions.

Assumption 1: The cable is inelastic and considered massless, and it is always tensioned during flight.

Assumption 2: The suspension point is coincident with the gravity center of the quadrotor UAV, and the behavior of the slung load is similar to a single-point spherical pendulum.

The dynamics of quadrotor UAV are formulated as follows [40]:

$$\begin{aligned}
\ddot{x}_e &= \left((F_r+F_f)(\cos\phi\sin\theta\cos\psi+\sin\phi\sin\psi)+F_x^L\right)/m_{qL}^n \\
\ddot{y}_e &= \left((F_r+F_f)(\sin\phi\sin\theta\cos\psi-\cos\phi\sin\psi)+F_y^L\right)/m_{qL}^n \\
\ddot{z}_e &= (F_r+F_f)\cos\phi\cos\theta/(m_q+m_L)-g+F_z^L/m_{qL}^n \\
\ddot{\phi} &= \dot{\theta}\dot{\psi}(J_y-J_z)/J_x+(T_\phi^r+T_\phi^f)/J_x+\tau_\phi^L/J_x \\
\ddot{\theta} &= \dot{\phi}\dot{\psi}(J_z-J_x)/J_y+(T_\theta^r+T_\theta^f)/J_y+\tau_\theta^L/J_y \\
\ddot{\psi} &= \dot{\phi}\dot{\theta}(J_x-J_y)/J_z+(T_\psi^r+T_\psi^f)/J_z+\tau_\psi^L/J_z
\end{aligned} \tag{1}$$

where x_e, y_e, and z_e represent the quadrotor UAV's position in the inertial frame $\{E\}$. ϕ,θ and ψ denote the roll, pitch and yaw Euler angles. J_x, J_y and J_z denote the moments of inertia along the respective airframe axis. m_{qL}^n is the nominal total mass and $m_{qL}^n = m_q + m_L^n$. m_q is the mass of quadrotor UAV. m_L^n is the nominal mass of suspended load and $\underline{m}_L \le m_L^n \le \overline{m}_L$. g is the gravitational acceleration. F_r is the desired total thrust of four propellers. F_f is the equivalent force induced by the additive actuator faults. T_ϕ^r, T_θ^r and T_ψ^r represent the desired torques. $\{F_x^L, F_y^L, F_z^L\}$ and $\{\tau_\phi^L, \tau_\theta^L, \tau_\psi^L\}$ represent the forces and torques exerted by the suspended load in the respective axis. T_ϕ^f, T_θ^f and T_ψ^f denote the equivalent fault torques.

$$\begin{aligned}
[F_r \quad T_\phi^r \quad T_\theta^r \quad T_\psi^r]^T &= K_{pwm}^F[u_{r1} \quad u_{r2} \quad u_{r3} \quad u_{r4}]^T \\
[F_f \quad T_\phi^f \quad T_\theta^f \quad T_\psi^f]^T &= K_{pwm}^F[f_1 \quad f_2 \quad f_3 \quad f_4]^T
\end{aligned} \tag{2}$$

where $u_{ri}, i=1,2,3,4$ is the reference motor pulse width modulation (PWM) input signal, $f_i, i=1,2,3,4$ is the equivalent motor PWM fault signal, and K_{pwm}^F is the mapping matrix between the generalized force and motor PWM signals.

Under Assumptions 1 and 2, the forces and torques exerted by the suspended load have the following specific forms[41].

$$\begin{aligned}
F_x &= m_L^n l(\ddot{\theta}_x\cos\theta_y\cos\theta_x-\dot{\theta}_x^2\cos\theta_y\cos\theta_x) \\
F_y &= m_L^n l(\ddot{\theta}_y\cos\theta_x\cos\theta_y-\dot{\theta}_y^2\cos\theta_x\sin\theta_y) \\
F_z &= m_L^n l(\ddot{\theta}_x\cos\theta_y\sin\theta_x+\dot{\theta}_x^2\cos\theta_y\cos\theta_x \\
&\quad +\ddot{\theta}_y\cos\theta_x\sin\theta_y+\dot{\theta}_y^2\cos\theta_x\cos\theta_y)-m_L^n g
\end{aligned} \tag{3}$$

where l is the length of the cable, and θ_x, θ_y are the suspension angles in the $x-z$ and $y-z$ planes, as shown in Fig. 1.

Remark 1. The equation (3) is obtained under the assumption that the load suspension point is coincident with the center of gravity and there are no torques applied to the body. In practice, the assumption is not satisfied. The torques $\tau_\phi^L, \tau_\theta^L, \tau_\psi^L$ caused by the load are not zero and it can be calculated based on an evaluation of offset between the gravity center and the suspension point.

Choosing altitude velocity and attitude angular velocity as states, and desired total thrust and equivalent torques as control inputs, the nonlinear state-space formulation of quadrotor UAV with additive faults is

$$\begin{aligned}
\dot{x} &= A(x)x+(B+\Delta B)u+Ff+Gg+Dd \\
y &= Cx+En
\end{aligned} \tag{4}$$

where $x=[\dot{z}_e \quad \dot{\phi} \quad \dot{\theta} \quad \dot{\psi}]^T$, $u=[F_r \quad T_\phi^r \quad T_\theta^r \quad T_\psi^r]^T$, $d=[F_z^L \quad \tau_\phi^L \quad \tau_\theta^L \quad \tau_\psi^L]^T$, $f=[f_1 \quad f_2 \quad f \quad f_4]^T$ is the additive fault, n is the measurement noise,

$$A=\begin{bmatrix} 0 & 0 & 0 & 0 \\ 0 & 0 & 0 & \dot{\theta}(J_y-J_z)/J_z \\ 0 & 0 & 0 & \dot{\phi}(J_z-J_x)/J_y \\ 0 & \dot{\theta}(J_x-J_y)/J_z & 0 & 0 \end{bmatrix},$$

$G=[1 \quad 0 \quad 0 \quad 0]^T$

$B=diag([1/m_{qL}^n \quad 1/J_x \quad 1/J_y \quad 1/J_z])$, $C=I$, $D=B$, $E=I$, $F=BK_{pwm}^F$.

Assumption 3: The initial state $x(0)$, the parameter uncertainty ΔB, and the disturbance d induced by the suspended load are unknown but bounded, satisfying $\underline{x}(0) \le x(0) \le \bar{x}(0)$, $\underline{\Delta B} \le \Delta B \le \overline{\Delta B}$ and $\underline{d} \le d \le \bar{d}$. Further, the boundaries $\underline{x}(0)$, $\bar{x}(0)$, $\underline{\Delta B}$, $\overline{\Delta B}$, $\underline{d}$ and $\bar{d}$ are all known.

Remark 2. Considering the coupling relationship between position x_e, y_e and attitude angles θ,ϕ, formulation (4), with altitude velocity and attitude angular velocity as states, can fully reflect the fault of four propeller motors.

B. LPV model for quadrotor UAV

To deal with the nonlinearity, the quadrotor UAV nonlinear model is converted into an LPV form, where the state space matrices depend affinely on the state vector. The detailed LPV form is set based on the work of [19]. Considering that the angular velocity is real-time measurable and bounded, its boundaries are set as

$$\dot{\phi} \in [\underline{\dot{\phi}}, \bar{\dot{\phi}}], \dot{\theta} \in [\underline{\dot{\theta}}, \bar{\dot{\theta}}] \tag{5}$$

Hence, the LPV model is

$$\begin{aligned}
\dot{x} &= \sum_{i=1}^4 \alpha_i A_i x+(B+\Delta B)u+Ff+Dd+Gg \\
y &= Cx+En
\end{aligned} \tag{6}$$

where α_i is the weighting function of each subsystem and $\sum_{i=1}^4 \alpha_i = 1, \forall t > 0$.

$$\alpha_1 = \frac{\left|\dot{\phi}-\underline{\dot{\phi}}\right|\left|\dot{\theta}-\underline{\dot{\theta}}\right|}{\left|\bar{\dot{\phi}}-\underline{\dot{\phi}}\right|\left|\bar{\dot{\theta}}-\underline{\dot{\theta}}\right|}, \alpha_2 = \frac{\left|\dot{\phi}-\underline{\dot{\phi}}\right|\left|\dot{\theta}-\bar{\dot{\theta}}\right|}{\left|\bar{\dot{\phi}}-\underline{\dot{\phi}}\right|\left|\bar{\dot{\theta}}-\underline{\dot{\theta}}\right|},$$

$$\alpha_3 = \frac{\left|\dot{\phi}-\bar{\dot{\phi}}\right|\left|\dot{\theta}-\underline{\dot{\theta}}\right|}{\left|\bar{\dot{\phi}}-\underline{\dot{\phi}}\right|\left|\bar{\dot{\theta}}-\underline{\dot{\theta}}\right|}, \alpha_4 = \frac{\left|\dot{\phi}-\bar{\dot{\phi}}\right|\left|\dot{\theta}-\bar{\dot{\theta}}\right|}{\left|\bar{\dot{\phi}}-\underline{\dot{\phi}}\right|\left|\bar{\dot{\theta}}-\underline{\dot{\theta}}\right|}$$

III. Actuator Fault Detection and Isolation

A. Fault detection and isolation scheme

The proposed actuator FDI scheme is depicted in Fig. 2. First, based on the quadrotor LPV model, a bank of H_- / H_∞ interval observers is designed, and the preliminary permissible upper and lower boundaries of states are obtained, which considers the effects of suspended load and parameter uncertainty on the system dynamics. Then, considering the effect of variable wind disturbance, a novel boundary update strategy based on residuals boundary and time window is proposed to adaptively adjust the state boundaries. The final decision formula of FDI is expressed as follows.

$$\begin{cases} y_i \in [\underline{\hat{y}}_{k,i}, \overline{\hat{y}}_{k,i}], \forall i = 1,2,3,4, \text{ Healthy} \\ y_i \notin [\underline{\hat{y}}_{k,i}, \overline{\hat{y}}_{k,i}], \exists i = 1,2,3,4, \text{ The } k\text{th actuator is faulty} \end{cases} \tag{7}$$

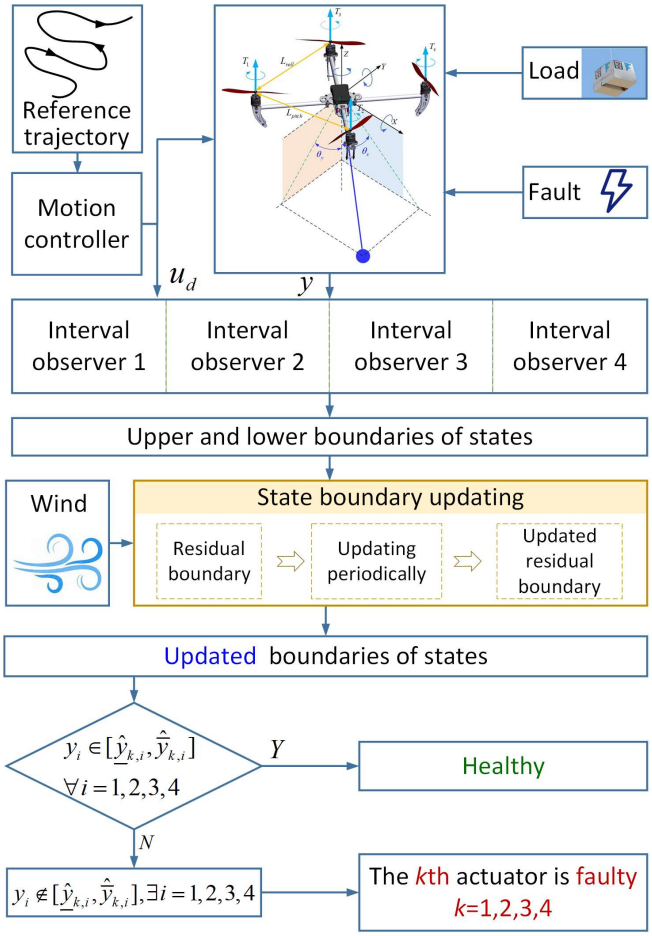

Fig. 2. The actuator FDI scheme

B. Boundary updating strategy

The preliminary state boundary is generated through the designed interval observer bank. Further, it will be adjusted periodically by the proposed updating strategy based on residuals and time windows. Define the residual $r_k = \hat{y}_k - y$, where the subscript k indicates that it corresponds to the actuator k, and $\hat{y}_k$ is the estimated output obtained by the kth interval observer. The updating of the states boundary is performed based on the updating of the residuals boundary, and the main workflow and steps are shown in Fig. 3 and Algorithm 1.

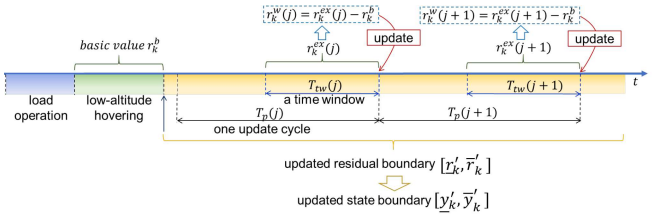

Fig. 3. The boundary update schematic diagram

Algorithm 1: Boundary updating of the kth observer

1: **Initialization**:
set the update period T_p and time-window T_{tw}
2: **Input**:
residual boundary r_k obtained by interval observers, the basic value r_k^b
3: **Repeat** (in the jth cycle $T_p(j)$)
4: **If** there are no fault alarms, **do it** in parallel
5: at the beginning of each cycle, update the residual boundary $r_k(j)$ using $r_k^w(j-1)$ of the previous cycle, and $r_k'(j) = r_k(j) - r_k^w(j-1)$
6: calculate the extreme value $r_k^{ex}(j)$ of the preliminary residual boundary $r_k(j)$ within a time window, and get the difference $r_k^w(j) = r_k^{ex}(j) - r_k^b$
7: **Output**: updated residual boundary r_k'

In the initialization, the values of the updating cycle T_p and time window T_{tw} are set based on the application scenario. After loading the cargo, the first step is to perform a low altitude hovering to obtain the base residual boundary. In the low-altitude hovering stage, where the effect of wind disturbance can be considered minimal, the mean of residual boundary over time is recorded and set as the base boundary r_k^b. At the beginning of each cycle, the preliminary residual boundary $r_k(j)$ is updated using $r_k^w(j-1)$, which is the evaluation of the effects of wind disturbance obtained in the previous cycle, and the updated residual boundary is $r_k'(j) = r_k(j) - r_k^w(j-1)$. Meanwhile, the preliminary residual boundary $r_k(j)$ within a time window is recorded and its extreme value is calculated as $r_k^{ex}(j) = [\min(\overline{r}_k(j))^T \quad \max(\underline{r}_k(j))^T]^T$. The difference with the base boundary r_k^b is served as an evaluation of the effect of wind disturbance, and $r_k^w(j) = r_k^{ex}(j) - r_k^b$. According to the updated residual boundary r_k', the final state boundaries for fault detection and isolation are $\hat{y}_k' = r_k' + y$.

***Remark* 3.** The application scenario of the boundary updating strategy is regular weather conditions, where the wind field shows a relatively smooth and stable variation trend. Thus, the effect of wind disturbance from the previous cycle is used to update the residual boundary of the current cycle. Moreover, the update period T_p and time window T_{tw} satisfy $0.5T_p \le T_{tw} \le T_p$, and their settings need to combine with the wind variations of practical scenarios. The faster the ambient wind changes, the smaller the value of the update cycle T_p.

***Remark* 4.** To ensure the normal execution of FDI, once a fault is detected, the corresponding updating algorithm stops running, and $\hat{y}_k' = \hat{y}_k$. It works again until the fault alarm is cleared.

***Remark* 5.** Effective application of the proposed boundary updating strategy requires that the actuators are healthy during cargo loading and low-altitude hovering.

C. FDI interval observer design

Based on the quadrotor LPV model (6), the interval observer is designed as:

$$\begin{aligned}
\dot{\hat{\bar{\xi}}} &= \sum_{i=1}^{4}\alpha_i(TA_i - \bar{L}_iC)\hat{\bar{x}} + TBu + \bar{L}y + TGg + \bar{\Theta}_0 + \bar{\chi}_0\\
\dot{\hat{\underline{\xi}}} &= \sum_{i=1}^{4}\alpha_i(TA_i - \underline{L}_iC)\hat{\underline{x}} + TBu + \underline{L}y + TGg + \underline{\Theta}_0 + \underline{\chi}_0\\
\hat{\bar{x}} &= \hat{\bar{\xi}} + Ny\\
\hat{\underline{x}} &= \hat{\underline{\xi}} + Ny\\
\hat{\bar{y}} &= C\hat{\bar{x}}\\
\hat{\underline{y}} &= C\hat{\underline{x}}
\end{aligned} \tag{8}$$

where $\bar{\Theta}_0 = (TD)^+\bar{d} - (TD)^-\underline{d}$, $\underline{\Theta}_0 = (TD)^+\underline{d} - (TD)^-\bar{d}$

$\bar{\chi}_0 = T^+(\overline{\Delta B}u^+ - \underline{\Delta B}u^-) - T^-(\underline{\Delta B}u^+ - \overline{\Delta B}u^-)$, and

$\underline{\chi}_0 = T^+(\underline{\Delta B}u^+ - \overline{\Delta B}u^-) - T^-(\overline{\Delta B}u^+ - \underline{\Delta B}u^-)$.

T and N are dimensionally appropriate matrices satisfying

$$T + NC = I \tag{9}$$

The residuals are defined as

$$\begin{aligned}
\bar{r} &= \hat{\bar{y}} - y\\
\underline{r} &= \hat{\underline{y}} - y
\end{aligned} \tag{10}$$

Define the estimation errors

$$\begin{aligned}
\bar{e} &= \hat{\bar{x}} - x\\
\underline{e} &= \hat{\underline{x}} - x
\end{aligned} \tag{11}$$

the error dynamic is

$$\begin{aligned}
\dot{\bar{e}} &= \sum_{i=1}^{4}(TA_i - \bar{L}_iC)e + \bar{L}_iEn + NE\dot{n} - TFf + \bar{\Theta} + \bar{\chi}\\
\dot{\underline{e}} &= \sum_{i=1}^{4}(TA_i - \underline{L}_iC)e + \underline{L}_iEn + NE\dot{n} - TFf + \underline{\Theta} + \underline{\chi}\\
\bar{r} &= C\bar{e} - En\\
\underline{r} &= C\underline{e} - En
\end{aligned} \tag{12}$$

where $\bar{\Theta} = \bar{\Theta}_0 - TDd$, $\underline{\Theta} = \underline{\Theta}_0 - TDd$, $\bar{\chi} = \bar{\chi}_0 - T\Delta Bu$, and $\underline{\chi} = \underline{\chi}_0 - T\Delta Bu$.

In the error dynamic system (12), TFf can be rewritten as

$$TFf = TF_kf_k + TF_k'f_k' \tag{13}$$

where F_k is the kth column of the fault matrix F, and F_k' is the remaining three columns of F. In the kth interval observer, the matrix T_k is selected satisfying

$$T_kF_k' = 0 \tag{14}$$

Thus, the kth interval observer is only sensitive to the kth actuator fault, achieving fault isolation.

Substituting

$$T_k = I - N_kC \tag{15}$$

into (14), it can be obtained that

$$F_k' = N_kCF_k' \tag{16}$$

It is assumed that $rank(F_k') = rank(CF_k')$ is satisfied.

Given matrices $\mathcal{V} \in \mathbb{R}^{n\times m}$, $\mathcal{M} \in \mathbb{R}^{m\times p}$ and $\mathcal{N} \in \mathbb{R}^{n\times p}$ with $rank(\mathcal{M}) = p$, the general solution $\mathcal{V}$ of the equation $\mathcal{V}\mathcal{M} = \mathcal{N}$ is [42]:

$$\mathcal{V} = \mathcal{N}\mathcal{M}^\dagger + \mathcal{S}(\mathcal{I} - \mathcal{M}\mathcal{M}^\dagger) \tag{17}$$

Thus, the general solution N_k of (16) is

$$N_k = F_k'(CF_k')^\dagger + \mathcal{S}_k\left(I - CF_k'(CF_k')^\dagger\right) \tag{18}$$

where $\mathcal{S}_k$ is an arbitrarily chosen matrix. It should be chosen such that $(T_kA_i, C), i = 1,2,3,4$ is detectable, and meanwhile, it should satisfy $rank(T_kF_k) = rank(F_k)$ such that the kth observer is sensitive to the kth actuator fault.

Therefore, the interval observer to locate the kth actuator fault is set as:

$$\begin{aligned}
\dot{\hat{\bar{\xi}}}_k &= \sum_{i=1}^{4}\alpha_i(T_kA_i - \bar{L}_{k,i}C)\hat{\bar{x}} + T_kBu + \bar{L}_{k,i}y + T_kGg + \bar{\Theta}_{k0} + \bar{\chi}_{k0}\\
\dot{\hat{\underline{\xi}}}_k &= \sum_{i=1}^{4}\alpha_i(T_kA_i - \underline{L}_{k,i}C)\hat{\underline{x}} + T_kBu + \underline{L}_{k,i}y + T_kGg + \underline{\Theta}_{k0} + \underline{\chi}_{k0}\\
\hat{\bar{x}}_k &= \hat{\bar{\xi}}_k + N_ky, \hat{\bar{y}}_k = C\hat{\bar{x}}_k\\
\hat{\underline{x}}_k &= \hat{\underline{\xi}}_k + N_ky, \hat{\underline{y}}_k = C\hat{\underline{x}}_k\\
\bar{r}_k &= \hat{\bar{y}}_k - y\\
\underline{r}_k &= \hat{\underline{y}}_k - y
\end{aligned} \tag{19}$$

where $\bar{\Theta}_{k0} = (T_kD)^+\bar{d} - (T_kD)^-\underline{d}$, $\underline{\Theta}_{k0} = (T_kD)^+\underline{d} - (T_kD)^-\bar{d}$

$\bar{\chi}_{k0} = T_k^+(\overline{\Delta B}u^+ - \underline{\Delta B}u^-) - T_k^-(\underline{\Delta B}u^+ - \overline{\Delta B}u^-)$, and

$\underline{\chi}_{k0} = T_k^+(\underline{\Delta B}u^+ - \overline{\Delta B}u^-) - T_k^-(\overline{\Delta B}u^+ - \underline{\Delta B}u^-)$.

The error dynamic of the kth interval observer is

$$\begin{aligned}
\dot{\overline{e}}_k &= \sum_{i=1}^{4}(T_kA_i - \overline{L}_{k,i}C)\overline{e}_k + \overline{L}_{k,i}En + N_kE\dot{n} - T_kF_kf + \overline{\Theta}_k + \overline{\chi}_k \\
\dot{\underline{e}}_k &= \sum_{i=1}^{4}(T_kA_i - \underline{L}_{k,i}C)\underline{e}_k + \underline{L}_{k,i}En + N_kE\dot{n} - T_kF_kf + \underline{\Theta}_k + \underline{\chi}_k \quad (20) \\
\overline{r}_k &= C\overline{e}_k - En \\
\underline{r}_k &= C\underline{e}_k - En
\end{aligned}$$

where $\overline{\Theta}_k = \overline{\Theta}_{k0} - T_kDd, \underline{\Theta}_k = \underline{\Theta}_{k0} - T_kDd$, $\overline{\chi}_k = \overline{\chi}_{k0} - T_k\Delta Bu$, and $\underline{\chi}_k = \underline{\chi}_{k0} - T_k\Delta Bu$.

Further, it can be concisely formulated as

$$\begin{aligned}
\dot{e}_k &= \sum\nolimits_{i=1}^{4}\tilde{A}_{Lk,i}e_k + \tilde{E}_{Lk,i}\tilde{n} + \tilde{F}_{Tk}\tilde{f} + \Omega_k \\
r_k &= \tilde{C}e_k + \tilde{E}\tilde{n}
\end{aligned} \quad (21)$$

where

$$e_k = \begin{bmatrix}\overline{e}_k \\ \underline{e}_k\end{bmatrix}, r_k = \begin{bmatrix}\overline{r}_k \\ \underline{r}_k\end{bmatrix}, \tilde{n} = \begin{bmatrix}n \\ \dot{n}\end{bmatrix}, \tilde{f} = \begin{bmatrix}f \\ f\end{bmatrix}, \tilde{E}_{Lk} = \begin{bmatrix}\overline{L}_{k,i}E & N_kE \\ \underline{L}_{k,i}E & N_kE\end{bmatrix},$$

$$\tilde{A}_{Lk,i} = \begin{bmatrix}T_kA_i - \overline{L}_{k,i}C & 0 \\ 0 & T_kA_i - \underline{L}_{k,i}C\end{bmatrix}, \Omega_k = \begin{bmatrix}\overline{\Theta}_k + \overline{\chi}_k \\ \underline{\Theta}_k + \underline{\chi}_k\end{bmatrix},$$

$$\tilde{F}_{Tk} = \begin{bmatrix}-T_kF_k & 0 \\ 0 & -T_kF_k\end{bmatrix}, \tilde{C} = \begin{bmatrix}C & 0 \\ 0 & C\end{bmatrix}, \tilde{E} = \begin{bmatrix}-E & 0 \\ -E & 0\end{bmatrix}.$$

Next, the stability and nonnegativity of the error dynamic are proved. Temporarily disregarding the faults and measurement noise terms, the error dynamic system is

$$\begin{cases}
\dot{\overline{e}}_k = \sum_{i=1}^{4}(T_kA_i - \overline{L}_{k,i}C)\overline{e}_k + \overline{\Theta}_k + \overline{\chi}_k \\
\dot{\underline{e}}_k = \sum_{i=1}^{4}(T_kA_i - \underline{L}_{k,i}C)\underline{e}_k + \underline{\Theta}_k + \underline{\chi}_k
\end{cases} \quad (22)$$

Given a vector $\nu \in \mathbb{R}^n$ that satisfies $\underline{\nu} \le \nu \le \overline{\nu}$, if $M \in \mathbb{R}^{m\times n}$ is a constant matrix, then [30],

$$M^+\underline{\nu} - M^-\overline{\nu} \le M\nu \le M^+\overline{\nu} - M^-\underline{\nu} \quad (23)$$

if $M \in \mathbb{R}^{m\times n}$ is a matrix satisfies $\underline{M} \le M \le \overline{M}$, then

$$\begin{aligned}
&\underline{M}^+\underline{\nu}^+ - \overline{M}^+\underline{\nu}^- - \underline{M}^-\overline{\nu}^+ + \overline{M}^-\overline{\nu}^- \le \\
&M\nu \le \overline{M}^+\overline{\nu}^+ - \overline{M}^+\underline{\nu}^- - \underline{M}^-\overline{\nu}^+ + \underline{M}^-\underline{\nu}^-
\end{aligned} \quad (24)$$

Based on the above lemma, it is obvious that

$$\begin{aligned}
\overline{\Theta}_k &= (T_kD)^+\underline{d} - (T_kD)^-\overline{d} - T_kDd \ge 0 \\
\underline{\Theta}_k &= (T_kD)^+\underline{d} - (T_kD)^-\overline{d} - T_kDd \le 0
\end{aligned} \quad (25)$$

$$\begin{aligned}
\overline{\chi}_k &= T_k^+(\overline{\Delta B}u^+ - \underline{\Delta B}u^-) - T_k^-(\underline{\Delta B}u^+ - \overline{\Delta B}u^-) - T_k\Delta Bu \ge 0 \\
\underline{\chi}_k &= T_k^+(\underline{\Delta B}u^+ - \overline{\Delta B}u^-) - T_k^-(\overline{\Delta B}u^+ - \underline{\Delta B}u^-) - T_k\Delta Bu \le 0
\end{aligned} \quad (26)$$

In the system (22), if $T_kA_i - \overline{L}_{k,i}C$ and $T_kA_i - \underline{L}_{k,i}C$ is not only Metzler but also Hurwitz, $\overline{e}_k \ge 0$ and $\underline{e}_k \le 0$ hold [43]. Furthermore, if the effect of measurement noise and disturbance are attenuated to a lesser level, the following relations are equivalent.

(1) $\underline{e}_k \le 0, \overline{e}_k \ge 0$.

(2) $\hat{\underline{x}}_k \le x \le \hat{\overline{x}}_k$.

(3) $\underline{y}_k \le y_k \le \overline{y}_k$.

(4) $\underline{r}_k \le 0, \overline{r}_k \ge 0$.

Thus, the FDI decision formula (7) is equivalent to

$$\begin{cases}
0 \in [\hat{\underline{r}}_{k,i}, \hat{\overline{r}}_{k,i}], \forall i = 1,2,3,4, \text{ Healthy} \\
0 \notin [\hat{\underline{r}}_{k,i}, \hat{\overline{r}}_{k,i}], \exists i = 1,2,3,4, \text{ The } k\text{th actuator is faulty}
\end{cases} \quad (27)$$

***Remark* 6.** The calculation of state boundaries $[\underline{y}_k, \overline{y}_k]$ requires the use of specific boundary values of slung-load disturbance and parameter uncertainty. The parameter uncertainty is mainly induced by mass fluctuations of suspended load. $\Delta B = diag([(m_{qL}^n - m_{qL})/(m_{qL}^n m_{qL}), 0, 0, 0])$ where m_{qL} is the actual total mass, which can be calculated based on the mass variation range $[\underline{m}_L, \overline{m}_L]$ of the suspended load. d is mainly caused by the swaying of suspended loads during transportation. The force $[F_z^L \quad F_y^L \quad F_z^L]$ exerted on the quadrotor UAV can be obtained based on equation (3) when the load suspension point coincides with the gravity center, and further, the torques τ applied to the airframe are calculated based on the evaluation of offset r between the suspension point and gravity center, and $\tau^L = r \times [F_z^L \quad F_y^L \quad F_z^L]^T$. The boundaries can be tuned in practice by multiplying with a safety factor κ .

$$\underline{d} = \kappa\bullet\min\{[F_z^L \quad (\tau^L)^T]^T\}, \overline{d} = \kappa\bullet\max\{[F_z^L \quad (\tau^L)^T]^T\}$$

$$\underline{\Delta B} = \kappa\bullet\min\{diag([(m_{qL}^n - m_{qL})/(m_{qL}^n m_{qL}) \quad 0 \quad 0 \quad 0])\},$$

$$\overline{\Delta B} = \kappa\bullet\max\{diag([(m_{qL}^n - m_{qL})/(m_{qL}^n m_{qL}) \quad 0 \quad 0 \quad 0])\}.$$

The stability conditions of observers are given by the following theorem.

***Theorem* 1**. Given positive vector $\eta_k \in \mathbb{R}^{2n_x}$, real numbers a_k, b_k satisfied $a_kb_k < 0$, the system is asymptotically stable, if there exist positive definite diagonal matrix P_k , matrices $X_{k,i}, Y_{k,i}, i = 1,2,3,4$, such that

$$\begin{bmatrix}\Omega_{k,1} & 0 \\ 0 & \Omega_{k,2}\end{bmatrix} > 0, i = 1,2,3,4 \quad (28)$$

$$\begin{bmatrix}
\mathrm{He}(\Phi_{k,i,1}) & * & * & * \\
0 & \mathrm{He}(\Phi_{k,i,2}) & * & * \\
\Phi_{k,i,31} & 0 & \mathrm{He}(\Phi_{k,i,3}) & * \\
0 & \Phi_{k,i,42} & 0 & \mathrm{He}(\Phi_{k,i,4})
\end{bmatrix} < 0 \quad (29)$$

where,

$$\Omega_{k,1} = P_{k1}T_kA_i - \overline{X}_{k,i}C + diag(\eta_{k1})P_{k1}$$

$$\Omega_{k,2} = P_{k2}T_kA_i - \underline{X}_{k,i}C + diag(\eta_{k1})P_{k1}$$

$$\Phi_{k,i,1}=-\bar{X}_{k,i}b_kI,\Phi_{k,i,2}=-\underline{X}_{k,i}b_kI$$
$$\Phi_{k,i,3}=C^T\bar{Y}_{k,i}a_kI-(T_kA_i)^T\bar{X}_{k,i}a_kI$$
$$\Phi_{k,i,4}=C^T\underline{Y}_{k,i}a_kI-(T_kA_i)^T\underline{X}_{k,i}a_kI$$
$$\Phi_{k,i,31}=P_{k1}+(T_kA_i)^T\bar{X}_{k,i}b_kI-C^T\bar{Y}_{k,i}b_kI+\bar{X}_{k,i}^Ta_kI$$
$$\Phi_{k,i,42}=P_{k2}+(T_kA_i)^T\underline{X}_{k,i}b_kI-C^T\underline{Y}_{k,i}b_kI+\underline{X}_{k,i}^Ta_kI$$

The matrix $L_{k,i}$ can be determined by $L_{k,i}=(Y_{k,i}X_{k,i}^{-1})^T$.

Proof: Inequation (28) is equivalent to

$$P_k\tilde{A}_{Lk,i}+diag(\eta_k)P_k>0 \tag{30}$$

where $P_k=\begin{bmatrix}P_{k1}&0\\0&P_{k2}\end{bmatrix}$. $P_k>0$ and all its diagonal terms are positive. According to the definition of Metzler matrix in [28], $\tilde{A}_{Lk,i}$ is Metzler if condition (30) is satisfied. Metzler matrix $\tilde{A}_{Lk,i}$ is Hurwitz if there exists a positive definite diagonal matrix $P_k>0$ such that the following inequality holds [43].

$$P_k\tilde{A}_{Lk,i}+\tilde{A}_{Lk,i}^TP_k<0 \tag{31}$$

It is equivalent to

$$\begin{bmatrix}\tilde{A}_{Lk,i}\\I\end{bmatrix}^T\begin{bmatrix}0&P_k\\P_k&0\end{bmatrix}\begin{bmatrix}\tilde{A}_{Lk,i}\\I\end{bmatrix}<0 \tag{32}$$

Since that $a_kb_k<0$, it is obvious that

$$\begin{bmatrix}a_kI\\b_kI\end{bmatrix}^T\begin{bmatrix}0&P_k\\P_k&0\end{bmatrix}\begin{bmatrix}a_kI\\b_kI\end{bmatrix}<0 \tag{33}$$

It can be noted that

$$\begin{bmatrix}a_kI\\b_kI\end{bmatrix}^T\begin{bmatrix}b_kI\\-a_kI\end{bmatrix}=0,\ \begin{bmatrix}-I\\\tilde{A}_{Lk,i}^T\end{bmatrix}^T\begin{bmatrix}\tilde{A}_{Lk,i}\\I\end{bmatrix}=0.$$

According to the Projection lemma[44], (32) is equal to

$$\begin{bmatrix}0&P_k\\P_k&0\end{bmatrix}+\mathrm{He}\left(\begin{bmatrix}-I\\\tilde{A}_{Lk,i}{}^T\end{bmatrix}X_{k,i}\begin{bmatrix}b_kI\\-a_kI\end{bmatrix}^T\right)<0 \tag{34}$$

Define $X_{k,i}=P_kL_{k,i}$, $Y_{k,i}=L_{k,i}^TX_{k,i}$,

$$L_{k,i}=\begin{bmatrix}\bar{L}_{k,i}&0\\0&\underline{L}_{k,i}\end{bmatrix}\ X_{k,i}=\begin{bmatrix}\bar{X}_{k,i}&0\\0&\underline{X}_{k,i}\end{bmatrix}\ Y_{k,i}=\begin{bmatrix}\bar{Y}_{k,i}&0\\0&\underline{Y}_{k,i}\end{bmatrix}.$$

Substituting the specific form of $P_k,\tilde{A}_{Lk,i},X_{k,i}$ into (34), inequality (29) can be obtained.

Aiming to attenuate the effect of sensor noise as much as possible while enhancing sensitivity to faults, the H_∞/H_- performances are applied, and sufficient conditions are given in the following theorem.

***Theorem* 2**: Given the positive scalars γ,β, the error system (21) has the H_-/H_∞ performance, if there exist positive definite matrix P_{fk}, symmetric matrices P_{nk} and Q_{n_k}, ($Q_{n_k}>0$), $X_{k,i}$, $H_{1k,i},H_{2k,i},H_{3k,i},H_{4k,i},H_{5k,i},H_{6k,i},H_{7k,i},H_{8k,i},i=1,2,3,4$ such that the following inequalities hold.

$$\begin{bmatrix}
0&*&*&*&*&*&*&*\\
0&0&*&*&*&*&*&*\\
\Upsilon_{k,i,31}&0&\mathrm{He}(\Upsilon_{k,i,3})&*&*&*&*&*\\
0&\Upsilon_{k,i,42}&0&\mathrm{He}(\Upsilon_{k,i,4})&*&*&*&*\\
\bar{H}_{1k,i}&0&\Upsilon_{k,i,53}&0&\Upsilon_{k,i,5}&*&*&*\\
0&\underline{H}_{1k,i}&0&\Upsilon_{k,i,64}&0&\Upsilon_{k,i,6}&*&*\\
\Upsilon_{k,i,71}&0&\Upsilon_{k,i,73}&0&\bar{H}_{4k,i}^T&0&\Upsilon_{k,i,7}&*\\
0&\Upsilon_{k,i,82}&0&\Upsilon_{k,i,84}&0&\underline{H}_{4k,i}^T&0&\Upsilon_{k,i,8}
\end{bmatrix}<0 \tag{35}$$

$$\begin{bmatrix}
-\bar{Q}_{nk}&*&*&*&*&*&*&*\\
0&-\underline{Q}_{nk}&*&*&*&*&*&*\\
\Psi_{k,i,31}&0&\Psi_{k,i,3}&*&*&*&*&*\\
0&\Psi_{k,i,42}&0&\Psi_{k,i,4}&*&*&*&*\\
\bar{H}_{5k,i}&0&\Psi_{k,i,53}&0&\Psi_{k,i,5}&*&*&*\\
0&\underline{H}_{5k,i}&0&\Psi_{k,i,64}&0&\Psi_{k,i,6}&*&*\\
\Psi_{k,i,71}&0&\Psi_{k,i,73}&0&\Psi_{k,i,75}&0&\Psi_{k,i,7}&*\\
0&\Psi_{k,i,82}&0&\Psi_{k,i,84}&0&\Psi_{k,i,86}&0&\Psi_{k,i,8}
\end{bmatrix}<0 \tag{36}$$

$\Upsilon_{k,i,3}=\bar{Y}_{k,i}^TC+\bar{H}_{2k,i}^TC-\bar{X}_{k,i}^TT_kA_i$, $\Upsilon_{k,i,4}=\underline{Y}_{k,i}^TC+\underline{H}_{2k,i}^TC-\underline{X}_{k,i}^TT_kA_i$

$\Upsilon_{k,i,5}=-I+\mathrm{He}(\bar{H}_{3k,i})$,

$\Upsilon_{k,i,6}=-I+\mathrm{He}(\underline{H}_{3k,i})$

$\Upsilon_{k,i,7}=\beta^2I+2F_k^TT_k^T\bar{X}_{k,i}^TT_kF_k$,

$\Upsilon_{k,i,8}=\beta^2I+2F_k^TT_k^T\underline{X}_{k,i}^TT_kF_k$

$\Upsilon_{k,i,31}=\bar{P}_{fk}+\bar{X}_{k,i}^T+C^T\bar{H}_{1k,i}$,

$\Upsilon_{k,i,42}=\underline{P}_{fk}+\underline{X}_{k,i}^T+C^T\underline{H}_{1k,i}$

$\Upsilon_{k,i,53}=\bar{H}_{3k,i}^TC+\bar{H}_{2k,i}$

$\Upsilon_{k,i,64}=\underline{H}_{3k,i}^TC+\underline{H}_{2k,i}$

$\Upsilon_{k,i,71}=F_k^TT_k^T\bar{X}_{k,i}^T$,

$\Upsilon_{k,i,82}=F_k^TT_k^T\underline{X}_{k,i}^T$

$\Upsilon_{k,i,73}=F_k^TT_k^T\bar{Y}_{k,i}C-F_k^TT_k^T\bar{X}_{k,i}^TT_kA_i+\bar{H}_{4k,i}^TC+F_k^TT_k^T\bar{X}_{k,i}$

$\Upsilon_{k,i,84}=F_k^TT_k^T\underline{Y}_{k,i}C-F_k^TT_k^T\underline{X}_{k,i}^TT_kA_i+\underline{H}_{4k,i}^TC+F_k^TT_k^T\underline{X}_{k,i}$

$\Psi_{k,i,3}=-w_1w_2\bar{Q}_{nk}+\mathrm{He}\left(C^T\bar{Y}_{k,i}-(T_kA_i)^T\bar{X}_{k,i}-C^{+T}\bar{H}_{6k,i}\right)$

$\Psi_{k,i,4}=\mathrm{He}\left(C^T\underline{Y}_{k,i}-(T_kA_i)^T\underline{X}_{k,i}-C^T\underline{H}_{6k,i}\right)-w_1w_2\underline{Q}_{nk}$

$\Psi_{k,i,5}=I+\mathrm{He}(\bar{H}_{7k,i}),\Psi_{k,i,6}=I+\mathrm{He}(\underline{H}_{7k,i})$

$\Psi_{k,i,7}=-\gamma^2I+\mathrm{He}\left(E^T\bar{H}_{8k,i}-E^T\bar{Y}_{k,i}\right)$

$\Psi_{k,i,8}=-\gamma^2I+\mathrm{He}\left(E^T\underline{H}_{8k,i}-E^T\underline{Y}_{k,i}\right)$

$\Psi_{k,i,31}=\bar{P}_{nk}-jw_c\bar{Q}_{nk}-C^T\bar{H}_{5k,i}+\bar{X}_{k,i}^T$

$\Psi_{k,i,42}=\underline{P}_{nk}-jw_c\underline{Q}_{nk}-C^T\underline{H}_{5k,i}+\underline{X}_{k,i}^T$

$\Psi_{k,i,53}=\bar{H}_{6k,i}-\bar{H}_{7k,i}^TC,\Psi_{k,i,64}=\underline{H}_{6k,i}-\underline{H}_{7k,i}^TC$

$\Psi_{k,i,71}=E^T\bar{H}_{5k,i}+\bar{X}_{k,i}^T,\Psi_{k,i,82}=E^T\underline{H}_{5k,i}+\underline{X}_{k,i}^T$

$\Psi_{k,i,75}=E^T\bar{H}_{7k,i}+\bar{H}_{8k,i}^T,\Psi_{k,i,86}=E^T\underline{H}_{7k,i}+\underline{H}_{8k,i}^T$

$\Psi_{k,i,73}=-E^T\bar{Y}_{k,i}+E^T\bar{H}_{6k,i}+\bar{Y}_{k,i}^TC-\bar{X}_{k,i}^TT_kA_i-\bar{H}_{8k,i}^TC$

$\Psi_{k,i,84}=-E^T\underline{Y}_{k,i}+E^T\underline{H}_{6k,i}+\underline{Y}_{k,i}^TC-\underline{X}_{k,i}^TT_kA_i-\underline{H}_{8k,i}^TC$

Proof: The candidate Lyapunov function is set as

$$V_{fk}=e_k{}^TP_{fk}e_k \tag{37}$$

where $P_{fk}=\begin{bmatrix}\bar{P}_{fk}&0\\0&\underline{P}_{fk}\end{bmatrix}$.

$$\begin{aligned}\dot{V}_{fk} &= e_k^{\ T}(\tilde{A}_{Lk,i}^T P_{fk} + P_{fk}\tilde{A}_{Lk,i})e_k \\ &\quad + e_k^{\ T} P_{fk}\tilde{F}_{Tk} f_k + f_k^{\ T}\tilde{F}_{Tk}^T P_{fk} e_k < 0\end{aligned} \tag{38}$$

$$J_{fk} = \dot{V}_{fk} + \beta^2 f^T f - r_k^{\ T} r_k < 0 \tag{39}$$

Thus,

$$\begin{aligned}J_{fk} &= e_k^{\ T}(\tilde{A}_{Lk,i}^T P_{fk} + P_{fk}\tilde{A}_{Lk,i} - C^T C)e_k \\ &\quad + e_k^{\ T} P_{fk}\tilde{F}_{Tk} f + f^T \tilde{F}_{Tk}^T P_{fk} e_k + \beta^2 f^T f < 0\end{aligned} \tag{40}$$

Inequality (40) can be rewritten as

$$\begin{bmatrix} e_k \\ \tilde{f} \end{bmatrix}^T \begin{bmatrix} P_{fk}\tilde{A}_{Lk,i} + \tilde{A}_{Lk,i}^T P_{fk} - C^T C & P_{fk}\tilde{F}_{Tk} \\ \tilde{F}_{Tk}^T P_{fk} & \beta^2 I \end{bmatrix} \begin{bmatrix} e_k \\ \tilde{f} \end{bmatrix} < 0 \tag{41}$$

It is equal to

$$\begin{bmatrix} \tilde{A}_{Lk,i} & \tilde{F}_{Tk,} \\ I & 0 \end{bmatrix}^T \Xi_{k1} \begin{bmatrix} \tilde{A}_{Lk,i} & \tilde{F}_{Tk} \\ I & 0 \end{bmatrix} + \begin{bmatrix} \tilde{C} & 0 \\ 0 & I \end{bmatrix}^T \Pi_{k1} \begin{bmatrix} \tilde{C} & 0 \\ 0 & I \end{bmatrix} < 0 \tag{42}$$

where $\Xi_{k1} = \begin{bmatrix} 0 & P_{fk} \\ P_{fk} & 0 \end{bmatrix}$, $\Pi_{k1} = \begin{bmatrix} -I & 0 \\ 0 & \beta^2 I \end{bmatrix}$

It can be rewritten as

$$\begin{bmatrix} \tilde{A}_{Lk,i} & \tilde{F}_{Tk} \\ I & 0 \\ \tilde{C} & 0 \\ 0 & I \end{bmatrix}^T \begin{bmatrix} \Xi_{k1} & 0 \\ 0 & \Pi_{k1} \end{bmatrix} \begin{bmatrix} \tilde{A}_{Lk,i} & \tilde{F}_{Tk} \\ I & 0 \\ \tilde{C} & 0 \\ 0 & I \end{bmatrix} < 0 \tag{43}$$

It is clear that

$$\begin{bmatrix} \tilde{A}_{Lk,i}^T & I & \tilde{C}^T & 0 \\ \tilde{F}_{Tk}^T & 0 & 0 & I \end{bmatrix} \begin{bmatrix} I & -\tilde{A}_{Lk,i} & 0 & -\tilde{F}_{Tk} \\ 0 & -\tilde{C} & I & 0 \end{bmatrix}^T = 0 \tag{44}$$

Let $\ell_{1k,i} = \begin{bmatrix} I & -\tilde{A}_{Lk,i} & 0 & -\tilde{F}_{Tk} \\ 0 & -\tilde{C} & I & 0 \end{bmatrix}^T$, $\ell_{1k,i}^{\perp} = \begin{bmatrix} \tilde{A}_{Lk,i}^T & I & \tilde{C}^T & 0 \\ \tilde{F}_{Tk}^T & 0 & 0 & I \end{bmatrix}$,

inequality (43) can be redescribed as

$$\ell_{1k,i}^{\perp} \Lambda_{k1} \left(\ell_{1k,i}^{\perp}\right)^T < 0 \tag{45}$$

where $\Lambda_{k1} = \begin{bmatrix} \Xi_{k1} & 0 \\ 0 & \Pi_{k1} \end{bmatrix}$.

According to the *Finsler*'s Lemma [20], [45], inequality (45) is equivalent to

$$\Lambda_{k1} + \ell_{1k,i} S_{1k,i} + (\ell_{1k,i} S_{1k,i})^T < 0 \tag{46}$$

Choose

$$S_{1k,i} = \begin{bmatrix} 0 & X_{k,i} & 0 & X_{k,i} \\ H_{1k,i} & H_{2k,i} & H_{3k,i} & H_{4k,i} \end{bmatrix} \tag{47}$$

where $X_{k,i} = \begin{bmatrix} \bar{X}_{k,i} & 0 \\ 0 & \underline{X}_{k,i} \end{bmatrix}$, $H_{jk,i} = \begin{bmatrix} \bar{H}_{jk,i} & 0 \\ 0 & \underline{H}_{jk,i} \end{bmatrix}$, $j = 1,2,3,4$.

Expanding the condition (46), (35) can be obtained.

The sensor noise is in a range $[\omega_1, \omega_2]$, and Ξ_{k2}, Π_{k2} are chosen as

$$\Xi_{k2} = \begin{bmatrix} -Q_{nk} & P_{nk} + j\omega_c Q_{nk} \\ P_{nk} - j\omega_c Q_{nk} & -\omega_1\omega_2 Q_{nk} \end{bmatrix}, \Pi_{k2} = \begin{bmatrix} I & 0 \\ 0 & -\gamma^2 I \end{bmatrix} \tag{48}$$

where $\omega_c = (\omega_1 + \omega_2)/2$, $P_{nk} = \begin{bmatrix} \bar{P}_{nk} & 0 \\ 0 & \underline{P}_{nk} \end{bmatrix}, Q_{nk} = \begin{bmatrix} \bar{Q}_{nk} & 0 \\ 0 & \underline{Q}_{nk} \end{bmatrix}$.

According to the GKYP lemma [46], it can be obtained that

$$\begin{aligned}&\begin{bmatrix} \tilde{A}_{Lk,i} & \tilde{E}_{Lk} \\ I & 0 \end{bmatrix}^T \begin{bmatrix} -Q_{nk} & P_{nk} + j\omega_c Q_{nk} \\ P_{nk} - j\omega_c Q_{nk} & -\omega_1\omega_2 Q_{nk} \end{bmatrix} \begin{bmatrix} \tilde{A}_{Lk,i} & \tilde{E}_{Lk} \\ I & 0 \end{bmatrix} \\ &+ \begin{bmatrix} \tilde{C} & \tilde{E} \\ 0 & I \end{bmatrix}^T \begin{bmatrix} I & 0 \\ 0 & -\gamma^2 I \end{bmatrix} \begin{bmatrix} \tilde{C} & \tilde{E} \\ 0 & I \end{bmatrix} < 0\end{aligned} \tag{49}$$

(49) can be rewritten as

$$\begin{bmatrix} \tilde{A}_{Lk,i} & \tilde{E}_{Lk} \\ I & 0 \\ \tilde{C} & \tilde{E} \\ 0 & I \end{bmatrix} \begin{bmatrix} \Xi_{k2} & 0 \\ 0 & \Pi_{k2} \end{bmatrix} \begin{bmatrix} \tilde{A}_{Lk,i} & \tilde{E}_{Lk} \\ I & 0 \\ \tilde{C} & \tilde{E} \\ 0 & I \end{bmatrix}^T < 0 \tag{50}$$

It can be seen that

$$\begin{bmatrix} \tilde{A}_{Lk,i}^T & I & \tilde{C}^T & 0 \\ \tilde{E}_{Lk}^T & 0 & \tilde{E}^T & I \end{bmatrix} \begin{bmatrix} I & -\tilde{A}_{Lk,i} & 0 & -\tilde{E}_{Lk} \\ 0 & -\tilde{C} & I & -\tilde{E} \end{bmatrix}^T = 0 \tag{51}$$

Let $\ell_{2k,i} = \begin{bmatrix} I & -\tilde{A}_{Lk,i} & 0 & -\tilde{E}_{Lk} \\ 0 & -\tilde{C} & I & -\tilde{E} \end{bmatrix}^T$,

$\ell_{2k,i}^{\perp} = \begin{bmatrix} \tilde{A}_{Lk,i}^T & I & \tilde{C}^T & 0 \\ \tilde{E}_{Lk}^T & 0 & \tilde{E}^T & I \end{bmatrix}$,

Inequality (50) can be rewritten as

$$\ell_{2k,i}^{\perp} \Lambda_{k2} \left(\ell_{2k,i}^{\perp}\right)^T < 0 \tag{52}$$

where $\Lambda_{k2} = \begin{bmatrix} \Xi_{k2} & 0 \\ 0 & \Pi_{k2} \end{bmatrix}$

Similarly, according to Finsler's Lemma, (52) is equivalent to

$$\Lambda_{k2} + \ell_{2k,i} S_{2k,i} + \left(\ell_{2k,i} S_{2k,i}\right)^T < 0 \tag{53}$$

Choose

$$S_{2k,i} = \begin{bmatrix} 0 & X_{k,i} & 0 & X_{k,i} \\ H_{5k,i} & H_{6k,i} & H_{7k,i} & H_{8k,i} \end{bmatrix} \tag{54}$$

where $H_{jk,i} = \begin{bmatrix} \bar{H}_{jk,i} & 0 \\ 0 & \underline{H}_{jk,i} \end{bmatrix}, j = 5,6,7,8$.

Expanding the condition (53), (36) can be obtained, and the proof is end.

The main solution steps of the designed interval observers are as follows. First, choosing a suitable matrix $\mathcal{S}_k$, the matrices N_k, T_k are obtained by solving equations (18) and (15). Then, given positive scalars β, γ, positive vectors $\eta_k \in \mathbb{R}^{2n_x}$, and real numbers a_k, b_k, the matrices P_k, P_{fk}, P_{nk}, $Q_{n,k}, X_{k,i}, Y_{k,i}, H_{1k,i}, H_{2k,i}, H_{3k,i}, H_{4k,i}, H_{5k,i}, H_{6k,i}, H_{7k,i}, H_{8k,i}$ are obtained by solving the linear matrix inequalities (28), (29), (35), and (36). Finally, the observer gains $L_{k,i}$ can be calculated by

$$L_{k,i} = (Y_{k,i} X_{k,i}^{-1})^T \tag{55}$$

IV. EXPERIMENTAL VALIDATION

A. Experimental platform

The architecture of the quadrotor UAV experimental platform is shown in Fig. 4, which consists of an optical positioning system, *QDrone*, load, ground station, and router. The load is suspended on the bottom of the quadrotor UAV by a blue inelastic cable. The optical positioning system containing ten cameras can capture the position and attitude information of the quadrotor UAV, and the captured data are transmitted to the ground station via an exchanger. *QDrone* is equipped with an inertial measurement unit (IMU), a magnetometer, a barometer, and a dual-band wireless network card, which can capture airframe attitude information. Data information and control command transmission between quadrotor UAV *QDrone* and ground station are achieved through a *WiFi* wireless network.

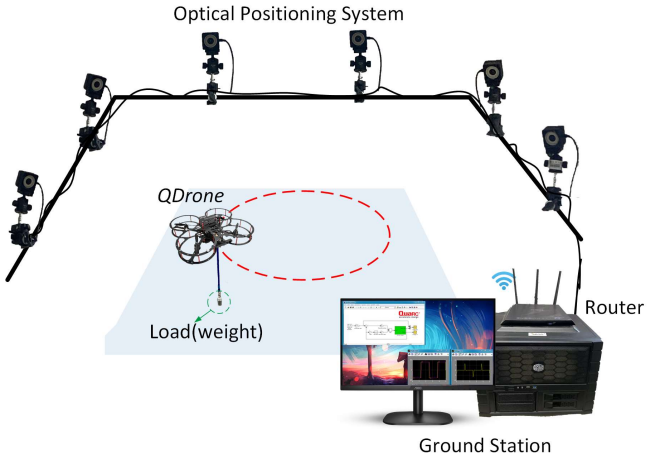

Fig. 4. The structure of the *QDrone* platform

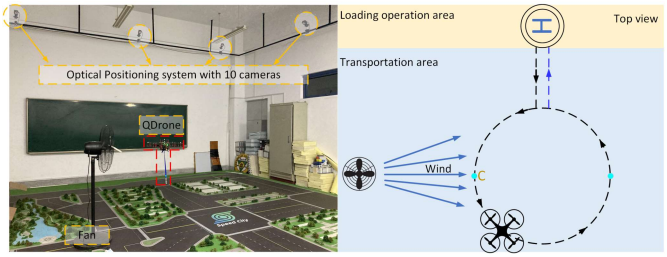

Fig. 5. Experimental scene setting

Tab. 1. Parameters of the *QDrone* quadrotor UAV

Notation	Parameters(unit)	value
K_f	the normalized lift coefficient (N)	5.11
K_t	the motor torque coefficient (Nm)	0.0487
m_q	total mass (kg)	1.121
g	gravity constant (m/s^2)	9.81
J_x	pitch moment of inertia (kgm^2)	1.0×10^{-2}
J_y	roll moment of inertia (kgm^2)	8.2×10^{-3}
J_z	yaw moment of inertia (kgm^2)	1.48×10^{-2}
L_{pitch}	pitch motor to motor distance (m)	0.2136
L_{roll}	roll motor to motor distance (m)	0.1758
l	the length of the cable (m)	0.4
m_L^n	the nominal mass of the load (kg)	0.075

The experimental scenario is shown in Fig. 5. The wind disturbance is exerted by an industrial fan in the transportation area, and there is no wind disturbance setup in the near-ground loading area. The parameter values of the quadrotor UAV are shown in Table 1.

The frequency of sensor noise is in the range of 0.01 Hz to 200 Hz. The parameters are set as

$$\beta=5,\gamma=1,\eta=10I,a=-5,b=2 \tag{56}$$

Combined with the experimental scenario set up in this paper, the sizes of the time window and update period are set as

$$T_{tw}=5s,T_p=10s \tag{57}$$

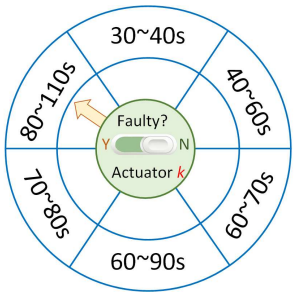

Fig. 6. Random fault setting

A random fault algorithm is designed, as shown in Fig. 6, which randomly determines whether an actuator is faulty and when it occurs. The amplitude of faults is

$$f_i=-0.2 \tag{58}$$

and the possible time ranges are also shown in Fig. 6.

***Remark* 7**. The updating period T_p and time window T_{tw} are set according to the wind field variation characteristics in the experimental scenarios, and they need to be tuned in different scenarios.

***Remark* 8**. The trajectory tracking of quadrotor UAV is realized by a PID controller, without taking fault-tolerance control actions.

B. FDI tests in fault-free case

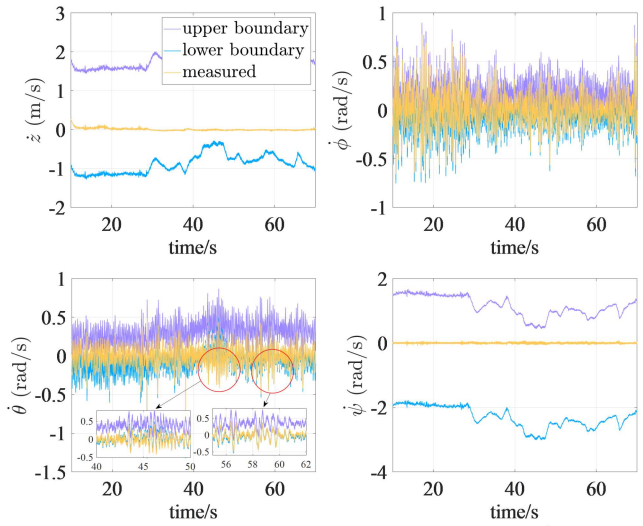

Fig. 7. Preliminary upper and lower boundaries of $\dot{\theta}$

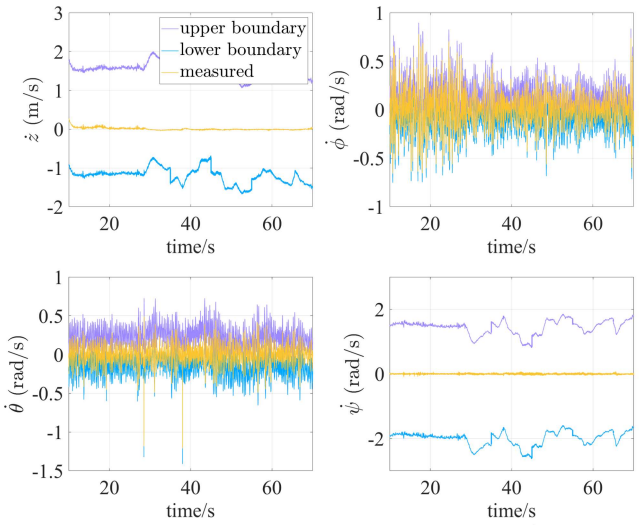

Fig. 8. Updated upper and lower boundaries of $\dot{\theta}$

Experiments in the scenario without setting faults but with wind are carried out to verify the effectiveness of the proposed boundary-updating strategy to cope with wind disturbance. Considering that the four observers differ only in their sensitive actuator faults and that the effect of wind disturbance is similar for each observer, the performance of the 3rd FDI observer is shown as an example.

In the experimental scenario with crosswind disturbance, the attitude is the first to be affected. Fig. 7 depicts the preliminary estimated interval generated by observer 3. Some of the measurements of pitch angular velocity $\dot{\theta}$ fall outside the estimated boundaries, as the quadrotor UAV passes through the region where the wind disturbance exists. This is because the effect of wind disturbance is not considered when generating preliminary state boundaries. According to the fault decision formulation (7), a fault alarm is triggered, as there exists one measured state that exceeds the estimated boundaries. The boundaries in Fig. 8 are updated. After adjusting the state boundaries through the proposed update strategy taking wind disturbance into account, the measured states are all within the updated boundaries.

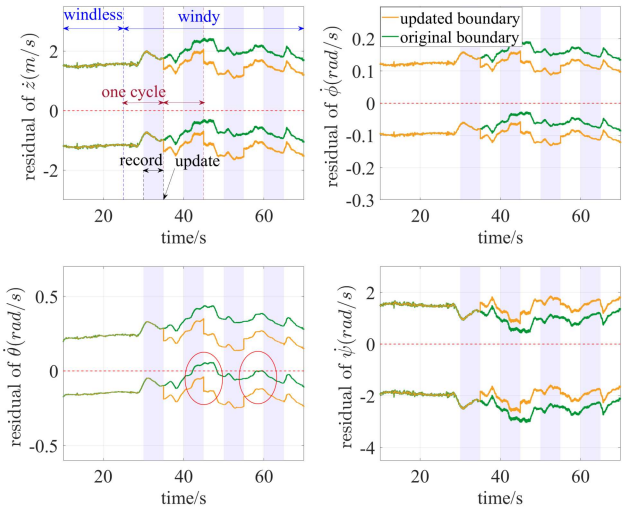

Fig. 9. Upper and lower boundaries of residual

The corresponding residual boundaries before and after updating are shown in Fig. 9.

The generated residual boundaries are smooth in the windless case, and the mean of the residual boundary over a period of time is taken as the base value r_k^b. The phase with a light purple fill indicates the time window, in which the variation of residual boundaries is recorded and the effect of wind disturbance is calculated. The green curves are the preliminary residual boundaries obtained by the interval observers, while the orange curves are the updated ones. In the boundaries before updating,

$$0 \notin [\underline{r}_{3,3}, \overline{r}_{3,3}], \text{when } 43s \le t \le 48s \tag{59}$$

which means a false alarm. While the updated orange boundaries avoid successfully the false alarm. Therefore, the proposed update strategy can cope well with wind disturbance effectively.

C. FDI tests under random faults

Experiments under random faults are carried out with a suspended load of $50g$ and $100g$, respectively. To present the performance of the proposed scheme more clearly, the FDI results are shown through residual boundaries.

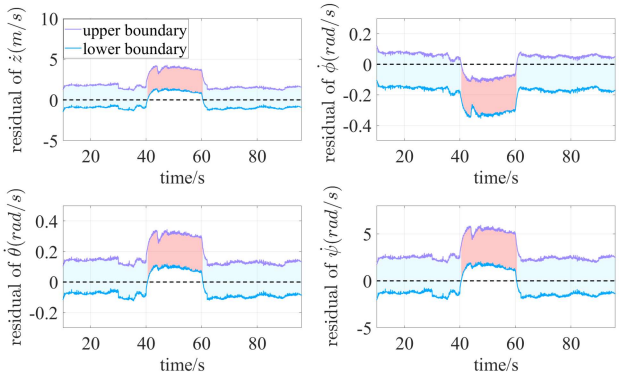

Fig. 10. Residual boundaries of observer 1 with a load of $50g$

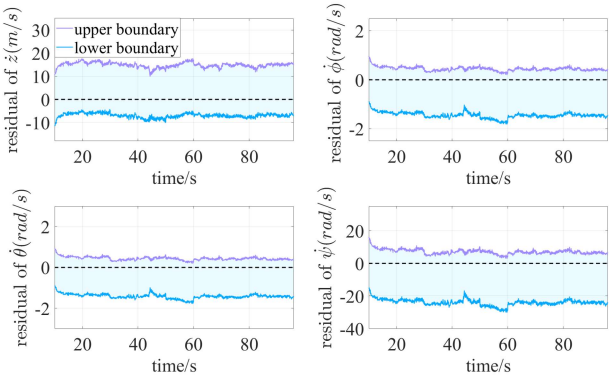

Fig. 11. Residual boundaries of observer 2 with a load of $50g$

Figs. 10 to 13 depict the residual boundaries corresponding to actuators 1 to 4, respectively, that are updated using the proposed strategy. The mass of the suspended load is $50g$. The light blue filled parts indicate that the measured states are within the estimated boundaries, and the actuator is healthy. While the red-filled part indicates that the measured states are outside the estimated boundaries, i.e., $0 \notin [\underline{r}_i, \overline{r}_i]$, implying the corresponding actuator is faulty.

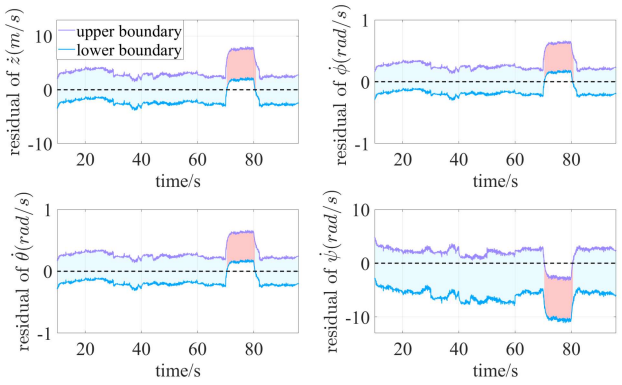

Fig. 12. Residual boundaries of observer 3 with a load of 50g

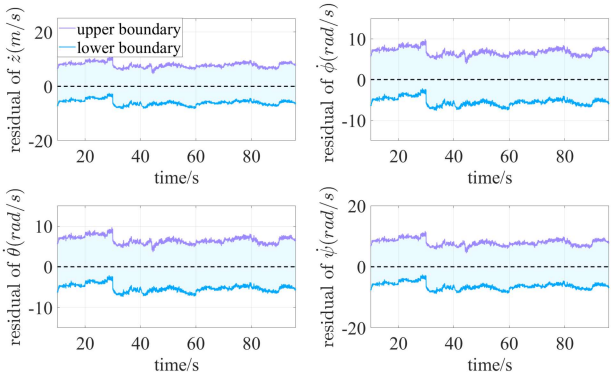

Fig. 13. Residual boundaries of observer 4 with a load of 50g

According to the FDI logical rules, it can be obtained that

$$\begin{cases} 0 \notin [\underline{r}_1, \overline{r}_1],\ 40.28s \le t \le 60.31s \\ 0 \notin [\underline{r}_3, \overline{r}_3],\ 70.35s \le t \le 80.26s \end{cases} \tag{60}$$

The data stored by the random fault algorithm is

$$\begin{cases} f_1 = -0.2, & 40s \le t \le 60s \\ f_3 = -0.2, & 70s \le t \le 80s \end{cases} \tag{61}$$

Comparison results show that the proposed method can accurately detect and locate faults within $0.2s$ to $0.4s$ after they occur, and there are no false alarms when passing through areas with wind disturbances.

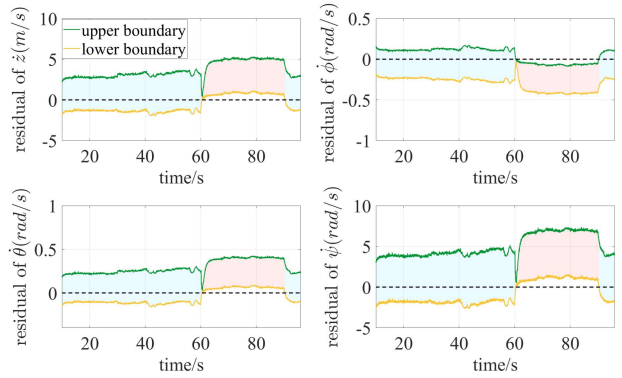

Fig. 14. Residual boundaries of observer 1 with a load of 100g

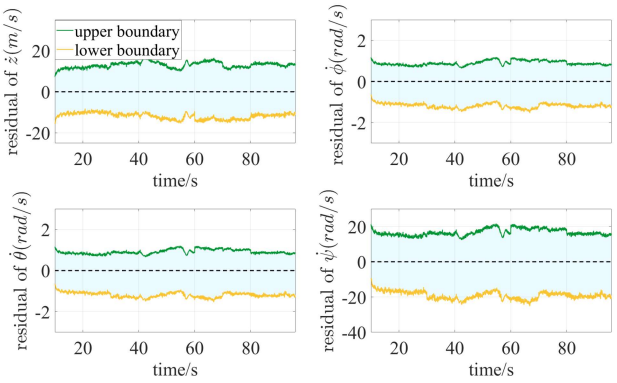

Fig. 15. Residual boundaries of observer 2 with a load of 100g

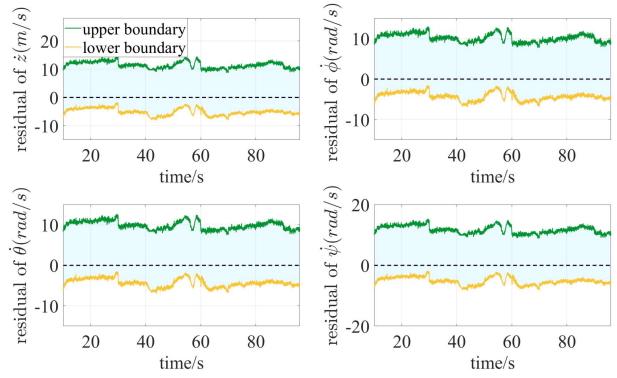

Fig. 16. Residual boundaries of observer 3 with a load of 100g

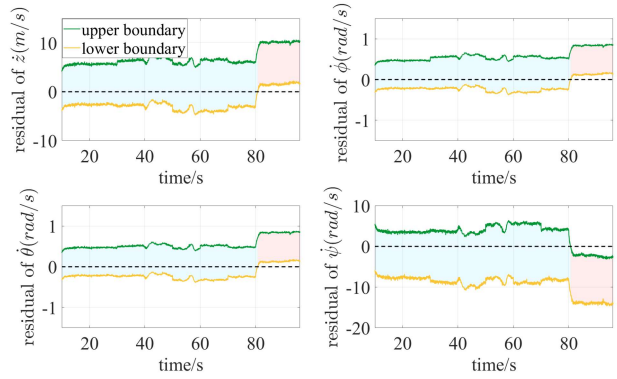

Fig. 17. Residual boundaries of observer 4 with a load of 100g

Figs. 14 to 17 depict the residual boundary curves of each actuator as the load mass increases to 100g. Similarly, the light blue-filled parts indicate that the measured states are within the estimated boundaries, i.e., $0 \in [\underline{r}_i, \overline{r}_i]$, while the red-filled part implies the corresponding actuator is faulty. It can be seen that

$$\begin{cases} 0 \notin [\underline{r}_1, \overline{r}_1], & 60.3s \le t \le 90.3s \\ 0 \notin [\underline{r}_4, \overline{r}_4], & 80.5s \le t \le 100s \end{cases} \tag{62}$$

The stored actuator fault setting is

$$\begin{cases} f_1 = -0.2, & 60s \le t \le 90s \\ f_4 = -0.2 & 80s \le t \le 100s \end{cases} \tag{63}$$

The faults are detected within 0.5s of occurrence. When the load mass increases, the proposed method is also able to detect and locate faults accurately. The results demonstrate that the proposed scheme can accurately detect and isolate actuator

faults in the presence of load mass fluctuations and wind disturbances.

V. Conclusion

In this paper, a state boundary estimation-based fault detection and isolation scheme is proposed. Based on the quadrotor LPV model, a bank of interval observers is designed, where H_- / H_∞ performances are applied to enhance sensitivity to faults and robustness to sensor noise. The preliminary upper and lower boundaries of states are generated by interval observers in fault-free cases, where the effects of parameter uncertainty and suspended load disturbance are included. Furthermore, considering the effects of varying wind disturbances, a novel strategy is proposed to adaptively adjust and update the state boundaries. Based on the *QDrone* platform, the effectiveness and performance of the proposed FDI scheme are demonstrated through experimental tests under random faults and variable mass loads. In future work, the safety control of quadrotor UAVs will be further explored.

References

[1] Y. Liu, Q. Wang, H. Hu, and Y. He, "A Novel Real-Time Moving Target Tracking and Path Planning System for a Quadrotor UAV in Unknown Unstructured Outdoor Scenes," *IEEE Transactions on Systems, Man, and Cybernetics: Systems*, vol. 49, no. 11, pp. 2362–2372, Nov. 2019, doi: 10.1109/TSMC.2018.2808471.

[2] Y. Zou and Z. Meng, "Immersion and Invariance-Based Adaptive Controller for Quadrotor Systems," *IEEE Transactions on Systems, Man, and Cybernetics: Systems*, vol. 49, no. 11, pp. 2288–2297, Nov. 2019, doi: 10.1109/TSMC.2018.2790929.

[3] G. Yu, D. Cabecinhas, R. Cunha, and C. Silvestre, "Aggressive maneuvers for a quadrotor-slung-load system through fast trajectory generation and tracking," *Auton. Robot.*, vol. 46, no. 4, pp. 499–513, Apr. 2022, doi: 10.1007/s10514-022-10035-y.

[4] G. Yu, J. Reis, D. Cabecinhas, R. Cunha, and C. Silvestre, "Reduced-Complexity Active Disturbance Rejection Controller for Quadrotor-Slung-Load Transportation," *IEEE Transactions on Systems, Man, and Cybernetics: Systems*, vol. 53, no. 8, pp. 5248–5259, Aug. 2023, doi: 10.1109/TSMC.2023.3263881.

[5] Y. Wang, G. Yu, W. Xie, W. Zhang, and C. Silvestre, "Cooperative Path Following Control of a Team of Quadrotor-Slung-Load Systems Under Disturbances," *IEEE Transactions on Intelligent Vehicles*, pp. 1–11, 2023, doi: 10.1109/TIV.2023.3274671.

[6] N. Wang, S.-F. Su, M. Han, and W.-H. Chen, "Backpropagating Constraints-Based Trajectory Tracking Control of a Quadrotor with Constrained Actuator Dynamics and Complex Unknowns," *IEEE Transactions on Systems, Man, and Cybernetics: Systems*, vol. 49, no. 7, pp. 1322–1337, Jul. 2019, doi: 10.1109/TSMC.2018.2834515.

[7] K. Rudin, G. J. J. Ducard, and R. Y. Siegwart, "Active Fault-Tolerant Control with Imperfect Fault Detection Information: Applications to UAVs," *IEEE Transactions on Aerospace and Electronic Systems*, vol. 56, no. 4, pp. 2792–2805, Aug. 2020, doi: 10.1109/TAES.2019.2959928.

[8] Z. Zhao, Y. Yang, S. X. Ding, and L. Li, "Fault-Tolerant Control for Systems with Model Uncertainty and Multiplicative Faults," *IEEE Trans. Syst. Man Cybern, Syst.*, vol. 50, no. 2, pp. 514–524, Feb. 2020, doi: 10.1109/TSMC.2017.2759144.

[9] Y. Hu, X. Dai, Y. Wu, B. Jiang, D. Cui, and Z. Jia, "Robust Fault Estimation and Fault-Tolerant Control for Discrete-Time Systems Subject to Periodic Disturbances," *IEEE Transactions on Circuits and Systems I: Regular Papers*, vol. 70, no. 7, pp. 2982–2994, Jul. 2023, doi: 10.1109/TCSI.2023.3268035.

[10] H. Zhang, Y. Mu, Z. Gao, and W. Wang, "Observer-Based Fault Reconstruction and Fault-Tolerant Control for Nonlinear Systems Subject to Simultaneous Actuator and Sensor Faults," *IEEE Transactions on Fuzzy Systems*, vol. 30, no. 8, pp. 2971–2980, Aug. 2022, doi: 10.1109/TFUZZ.2021.3098341.

[11] Z. Gao, C. Cecati, and S. X. Ding, "A Survey of Fault Diagnosis and Fault-Tolerant Techniques—Part I: Fault Diagnosis with Model-Based and Signal-Based Approaches," *IEEE Trans. Ind. Electron.*, vol. 62, no. 6, pp. 3757–3767, Jun. 2015, doi: 10.1109/TIE.2015.2417501.

[12] Y. Mu, H. Zhang, R. Xi, Z. Wang, and J. Sun, "Fault-Tolerant Control of Nonlinear Systems with Actuator and Sensor Faults Based on T–S Fuzzy Model and Fuzzy Observer," *IEEE Trans. Syst. Man Cybern, Syst.*, vol. 52, no. 9, pp. 5795–5804, Sep. 2022, doi: 10.1109/TSMC.2021.3131495.

[13] X. Wang, "Active Fault Tolerant Control for Unmanned Underwater Vehicle with Actuator Fault and Guaranteed Transient Performance," *IEEE Transactions on Intelligent Vehicles*, vol. 6, no. 3, pp. 470–479, Sep. 2021, doi: 10.1109/TIV.2020.3038785.

[14] A. Abbaspour, P. Aboutalebi, K. K. Yen, and A. Sargolzaei, "Neural adaptive observer-based sensor and actuator fault detection in nonlinear systems: Application in UAV," *ISA Transactions*, vol. 67, pp. 317–329, Mar. 2017, doi: 10.1016/j.isatra.2016.11.005.

[15] Z. Cen, H. Noura, T. B. Susilo, and Y. A. Younes, "Robust Fault Diagnosis for Quadrotor UAVs Using Adaptive Thau Observer," *J Intell Robot Syst*, vol. 73, no. 1–4, pp. 573–588, Jan. 2014, doi: 10.1007/s10846-013-9921-8.

[16] W. Han, Z. Wang, Y. Shen, and J. Qi, "L∞ Observer for Uncertain Linear Systems," *Asian Journal of Control*, vol. 21, no. 1, pp. 632–638, 2019, doi: 10.1002/asjc.1740.

[17] W. Han, Z. Wang, and Y. Shen, "H_/L∞ fault detection observer for linear parameter-varying systems with parametric uncertainty," *Int J Robust Nonlinear Control*, vol. 29, no. 10, pp. 2912–2926, Jul. 2019, doi: 10.1002/rnc.4530.

[18] M. Hou and R. J. Patton, "An LMI approach to H_/H∞ fault detection observers," *In Proceedings of the UKACC International Conference on Control*, pp. 305–310, Jan. 1996, doi: 10.1049/cp:19960570.

[19] L. Chen and R. J. Patton, "A time-domain LPV H_/H∞ fault detection filter," *IFAC-PapersOnLine*, vol. 50, no. 1, pp. 8600–8605, Jul. 2017, doi: 10.1016/j.ifacol.2017.08.1427.

[20] H. Zhang and J. Wang, "Active Steering Actuator Fault Detection for an Automatically-Steered Electric Ground Vehicle," *IEEE Transactions on Vehicular Technology*, vol. 66, no. 5, pp. 3685–3702, 2017, doi: 10.1109/TVT.2016.2604759.

[21] E. Chanthery, L. Travé-Massuyès, and S. Indra, "Fault Isolation on Request Based on Decentralized Residual Generation," *IEEE Transactions on Systems, Man, and Cybernetics: Systems*, vol. 46, no. 5, pp. 598–610, May 2016, doi: 10.1109/TSMC.2015.2479192.

[22] J. A. Guzmán-Rabasa, F. R. López-Estrada, B. M. González-Contreras, G. Valencia-Palomo, M. Chadli, and M. Pérez-Patricio, "Actuator fault detection and isolation on a quadrotor unmanned aerial vehicle modeled as a linear parameter-varying system," *Measurement and Control*, vol. 52, no. 9–10, pp. 1228–1239, Nov. 2019, doi: 10.1177/0020294018824764.

[23] F. R. López-Estrada, J.-C. Ponsart, D. Theilliol, Y. Zhang, and C.-M. Astorga-Zaragoza, "LPV Model-Based Tracking Control and Robust Sensor Fault Diagnosis for a Quadrotor UAV," *J Intell Robot Syst*, vol. 84, no. 1–4, pp. 163–177, Dec. 2016, doi: 10.1007/s10846-015-0295-y.

[24] H. Li, Q. Jia, R. Ma, and X. Chen, "Observer-based robust actuator fault isolation and identification for microsatellite attitude control systems," *Aircraft Engineering and Aerospace Technology*, vol. 93, no. 7, pp. 1145–1155, Jan. 2021, doi: 10.1108/AEAT-10-2020-0224.

[25] W. Han, H. L. Trentelman, and B. Xu, "Distributed H_/L∞ fault detection observer design for linear systems," *IFAC-PapersOnLine*, vol. 53, no. 2, pp. 688–693, 2020, doi: 10.1016/j.ifacol.2020.12.816.

[26] Y. Li, X. Zhu, and G. Yin, "Robust actuator fault detection for quadrotor UAV with guaranteed sensitivity," *Control Engineering Practice*, vol. 138, p. 105588, Sep. 2023, doi: 10.1016/j.conengprac.2023.105588.

[27] M. Chadli, A. Abdo, and S. X. Ding, "H_/H∞ fault detection filter design for discrete-time Takagi–Sugeno fuzzy system," *Automatica*, vol. 49, no. 7, pp. 1996–2005, Jul. 2013, doi: 10.1016/j.automatica.2013.03.014.

[28] T. Chevet, T. N. Dinh, J. Marzat, and T. Raïssi, "Robust Sensor Fault Detection for Linear Parameter-Varying Systems using Interval Observer," in *Proceedings of the 31st European Safety and Reliability Conference (ESREL 2021)*, Research Publishing Services, 2021, pp. 1486–1493. doi: 10.3850/978-981-18-2016-8_380-cd.

[29] F. Xu, V. Puig, C. Ocampo-Martinez, F. Stoican, and S. Olaru, "Improved Fault Detection and Isolation Strategy using a Bank of Interval Observers," *IFAC Proceedings Volumes*, vol. 47, no. 3, pp. 8024–8029, 2014, doi: 10.3182/20140824-6-ZA-1003.01651.

[30] R. Akremi, R. Lamouchi, M. Amairi, T. N. Dinh, and T. Raïssi, "Functional interval observer design for multivariable linear parameter-varying systems," *European Journal of Control*, vol. 71, p. 100794, May 2023, doi: 10.1016/j.ejcon.2023.100794.

[31] S. M. D. Oca and V. Puig, "Adaptive Threshold Generation for Robust Fault Detection using Interval LPV Observers," *IFAC Proceedings Volumes*, vol. 42, no. 8, pp. 444–449, 2009, doi: 10.3182/20090630-4-ES-2003.00074.

[32] M. Pourasghar, V. Puig, and C. Ocampo-Martinez, "Interval observer fault detection ensuring detectability and isolability by using a set-invariance approach," *IFAC-PapersOnLine*, vol. 51, no. 24, pp. 1111–1118, 2018, doi: 10.1016/j.ifacol.2018.09.727.

[33] Z.-H. Zhang and G.-H. Yang, "Distributed Fault Detection and Isolation for Multiagent Systems: An Interval Observer Approach," *IEEE Transactions on Systems, Man, and Cybernetics: Systems*, vol. 50, no. 6, pp. 2220–2230, Jun. 2020, doi: 10.1109/TSMC.2018.2811390.

[34] W. Tang, Z. Wang, Q. Zhang, and Y. Shen, "Set-membership estimation for linear time-varying descriptor systems," *Automatica*, vol. 115, p. 108867, May 2020, doi: 10.1016/j.automatica.2020.108867.

[35] Y. Ma, Z. Wang, N. Meslem, T. Raïssi, and Y. Shen, "Fault diagnosis by interval-based adaptive thresholds and peak-to-peak observers," *Adaptive Control & Signal*, vol. 37, no. 2, pp. 519–537, Feb. 2023, doi: 10.1002/acs.3535.

[36] E.-J. Pérez-Pérez, V. Puig, F.-R. López-Estrada, G. Valencia-Palomo, I. Santos-Ruiz, and S. E. Samada, "Fault detection and isolation in wind turbines based on neuro-fuzzy qLPV zonotopic observers," *Mechanical Systems and Signal Processing*, vol. 191, p. 110183, May 2023, doi: 10.1016/j.ymssp.2023.110183.

[37] L. Cao, X. Yang, G. Wang, Y. Liu, and Y. Hu, "Fault detection based on extended state observer and interval observer for UAVs," *Aircraft Engineering and Aerospace Technology*, vol. 94, no. 10, pp. 1759–1771, Jan. 2022, doi: 10.1108/AEAT-05-2021-0164.

[38] F. Zhu, Y. Tang, and Z. Wang, "Interval-Observer-Based Fault Detection and Isolation Design for T-S Fuzzy System Based on Zonotope Analysis," *IEEE Transactions on Fuzzy Systems*, vol. 30, no. 4, pp. 945–955, Apr. 2022, doi: 10.1109/TFUZZ.2021.3050854.

[39] Y. Lei, Y. Huang, and H. Wang, "Effects of Wind Disturbance on the Aerodynamic Performance of a Quadrotor MAV during Hovering," *Journal of Sensors*, vol. 2021, pp. 1–13, Apr. 2021, doi: 10.1155/2021/6681716.

[40] C. Li, Y. Wang, and X. Yang, "Adaptive fuzzy control of a quadrotor using disturbance observer," *Aerospace Science and Technology*, vol. 128, p. 107784, Sep. 2022, doi: 10.1016/j.ast.2022.107784.

[41] Ö. Bingöl and H. M. Güzey, "Neuro sliding mode control of quadrotor UAVs carrying suspended payload," *Advanced Robotics*, vol. 35, no. 3–4, pp. 255–266, Feb. 2021, doi: 10.1080/01691864.2020.1870557.

[42] Y. Wang, V. Puig, F. Xu, and G. Cembrano, "Robust fault detection and isolation based on zonotopic unknown input observers for discrete-time descriptor systems," *Journal of the Franklin Institute*, vol. 356, no. 10, pp. 5293–5314, Jul. 2019, doi: 10.1016/j.jfranklin.2019.04.014.

[43] D. Efimov and T. Raïssi, "Design of interval observers for uncertain dynamical systems," *Autom Remote Control*, vol. 77, no. 2, pp. 191–225, Feb. 2016, doi: 10.1134/S0005117916020016.

[44] P. Gahinet and P. Apkarian, "A linear matrix inequality approach to H∞ control," *Int. J. Robust Nonlinear Control*, vol. 4, no. 4, pp. 421–448, 1994, doi: 10.1002/rnc.4590040403.

[45] M. C. De Oliveira, "Investigating duality on stability conditions," *Systems & Control Letters*, vol. 52, no. 1, pp. 1–6, May 2004, doi: 10.1016/j.sysconle.2003.09.011.

[46] T. Iwasaki and S. Hara, "Generalized KYP lemma: unified frequency domain inequalities with design applications," *IEEE Transactions on Automatic Control*, vol. 50, no. 1, pp. 41–59, Jan. 2005, doi: 10.1109/TAC.2004.840475.

Xiaoyuan Zhu (Member, IEEE) received the B.E. and Ph.D. degree in Mechanical Engineering from Northwestern Polytechnical University, Xi'an, China, in 2009 and 2015, respectively. During 2012-2014, he was a visiting scholar in Department of Mechanical and Aerospace Engineering, the Ohio State University, Columbus, Ohio, USA. He is now an Associated Professor with the School of Mechanical Engineering, Southeast University, China. He serves as Member of *SAE New Energy Vehicles Technical Committee*, Editorial Board Member of *Cyber-Physical Systems*. His current research interests include electrified powertrain system and control, intelligent unmanned system, fault diagnosis and health management.

Yuxue Li received the B.E. degree in Mechanical Engineering from Southeast University, Nanjing, China, in 2021. She is currently pursuing the M.S. degree in Mechanical Engineering at Southeast University. Her research interests include fault diagnosis and fault tolerant control, UAV system.

Guodong Yin (Senior Member, IEEE) received the Ph.D. degree in mechanical engineering from Southeast University, Nanjing, China, in 2007. From August 2011 to August 2012, he was a Visiting Scholar with the Department of Mechanical and Aerospace Engineering, Ohio State University, Columbus, OH, USA. He is currently a Professor with the School of Mechanical Engineering, Southeast University, Nanjing, China. His research interests include automated vehicles, vehicle dynamics and control, and connected vehicles. He was the recipient of the National Science Fund for Distinguished Young Scholars.

Ron J. Patton (Life Fellow, IEEE) received the B Eng, M Eng, and PhD degrees in Electrical and Electronic Engineering and Control Systems from the University of Sheffield, UK, in 1971, 1974, and 1980, respectively. He is currently the Chair of Control and Intelligent Systems Engineering at Hull University, UK. He has made a substantial contribution to the field of modeling and design of robust methods for fault detection and isolation and fault-tolerant control (FTC) in dynamic systems as the author of 376 papers, including 147 journal papers and 7 books, with h-index 63. His current research interests include robust, multiple-model, and decentralized control strategies for FTC systems and applications in marine renewable energy and aerospace systems. Prof. Patton is Fellow of the IEEE, Senior Member of AIAA and Fellow of the Institute of Measurement and Control.